OPTICS

Table-top extreme ultraviolet second harmonic generation

Tobias Helk[1,2*†], Emma Berger[3,4†], Sasawat Jamnuch[5†], Lars Hoffmann[6], Adeline Kabacinski[7], Julien Gautier[7], Fabien Tissandier[7], Jean-Philipe Goddet[7], Hung-Tzu Chang[3], Juwon Oh[3], C. Das Pemmaraju[8], Tod A. Pascal[5,9,10], Stephane Sebban[7], Christian Spielmann[1,2*], Michael Zuerch[1,3,4,6*]

The lack of available table-top extreme ultraviolet (XUV) sources with high enough fluxes and coherence properties has limited the availability of nonlinear XUV and x-ray spectroscopies to free-electron lasers (FELs). Here, we demonstrate second harmonic generation (SHG) on a table-top XUV source by observing SHG near the Ti $M_{2,3}$ edge with a high-harmonic seeded soft x-ray laser. Furthermore, this experiment represents the first SHG experiment in the XUV. First-principles electronic structure calculations suggest the surface specificity and separate the observed signal into its resonant and nonresonant contributions. The realization of XUV-SHG on a table-top source opens up more accessible opportunities for the study of element-specific dynamics in multicomponent systems where surface, interfacial, and bulk-phase asymmetries play a driving role.

INTRODUCTION

Nonlinear interactions between light and matter not only form the basis for the generation of light at wavelengths spanning the terahertz to x-ray regimes but also enable spectroscopies that yield unique insight into fundamental material properties (*1*–*3*). When describing the nonlinear light-matter interaction, a material's polarization response to incident light of frequency ω can be approximated as a power series in increasing powers of the electric field $E(\omega)$, where only noncentrosymmetric materials, interfaces, and surfaces permit nonvanishing even-order terms. For this reason, second harmonic generation (SHG) and sum-frequency generation (SFG) are inherently sensitive to broken inversion symmetry (*4*, *5*). Up to a constant factor, the frequency-dependent effective second-order nonlinear-susceptibility $\chi^{(2)}$ can be extracted experimentally via the relationship

$$I(2\omega) \propto |\chi^{(2)}(2\omega;\omega+\omega)|^2 I(\omega)^2 \quad (1)$$

where $I(\omega)$ is the intensity at frequency ω. While optical nonlinear spectroscopies have been highly insightful probes of interfacial chemistry (*6*–*9*) and broken symmetries in solid-state systems (*10*), optical light can couple efficiently to multiple excitation pathways, rendering spectra difficult to interpret in multi-element samples (*11*, *12*). The desire to gain core-level specificity in nonlinear spectroscopies is thus motivated by the study of complex systems with wide-ranging applications including all-solid-state batteries with multiple buried interfaces, ferroelectric materials that, by definition, have bulk-phase structural asymmetries, and low-dimensional heterostructures, to name a few examples.

Popular element-specific probing methods include photoelectron and linear x-ray spectroscopies, which are sensitive to either surface or bulk properties, respectively, but not both, prompting recent efforts to apply nonlinear spectroscopies to the x-ray regime (*13*). The first promising experiments at free-electron lasers (FELs) have demonstrated soft x-ray (SXR) SHG as a viable technique to study noncentrosymmetric materials (*14*–*16*), surfaces (*17*), and buried organic-inorganic interfaces (*18*) when the energy of the fundamental or its SHG counterpart matches an allowed electronic transition. With FEL sources, the inherent intensity jitter lends itself naturally to calculating the nonlinear response via Eq. 1. The next frontier in x-ray SHG lies in the development of compact table-top sources capable of delivering high enough x-ray photon fluxes for nonlinear techniques. Given the moderate input intensities (~10^{12} W/cm^2) required for FEL-SHG that are in line with numerical estimations of intensities required for two-photon absorption (*19*), it is not unreasonable to think that high-power table-top HHG (high harmonic generation)-based sources could be used in a similar scheme (*17*, *20*–*23*).

Here, we report the first extreme ultraviolet second harmonic generation (XUV-SHG) experiment above the Ti M edge (32.6 eV), which also represents the first table-top demonstration of SHG at photon energies beyond the UV regime. A comparison of our observations with density functional perturbation theory (DFPT) and real-time time-dependent density functional theory (RT-TDDFT) calculations suggests resonant contributions to SHG from Ti-3p to Ti-3d transitions at the Ti surface. This proof-of-concept experiment demonstrating XUV-SHG aims to present on viable parameter ranges that will enable XUV-SHG at similar high-flux table-top sources.

RESULTS

In the experimental setup depicted in Fig. 1A, a 37.8-eV HHG-SXRL (soft x-ray laser) (*20*, *24*) with an average input energy of 111 ± 23 nJ, pulse duration of 1.73 ± 0.13 ps, and Gaussian-like beam profile

[1]Institute of Optics and Quantum Electronics, Abbe Center of Photonics, Friedrich-Schiller University, 07743 Jena, Germany. [2]Helmholtz Institute Jena, 07743 Jena, Germany. [3]Department of Chemistry, University of California, Berkeley, Berkeley, CA 94720, USA. [4]Materials Science Division, Lawrence Berkeley National Laboratory, Berkeley, CA 94720, USA. [5]ATLAS Materials Physics Laboratory, Department of NanoEngineering and Chemical Engineering, University of California, San Diego, La Jolla, CA 92023, USA. [6]Fritz Haber Institute of the Max Planck Society, 14195 Berlin, Germany. [7]Laboratoire d'Optique Appliquée, ENSTA Paris, Ecole Polytechnique, CNRS, Institut Polytechnique de Paris, Palaiseau, France. [8]Stanford Institute for Materials and Energy Sciences, SLAC National Accelerator Laboratory, Stanford, CA 94025, USA. [9]Materials Science and Engineering, University of California, San Diego, La Jolla, CA 92023, USA. [10]Sustainable Power and Energy Center, University of California, San Diego, La Jolla, CA 92023, USA.
*Corresponding author. Email: tobias.helk@uni-jena.de (T.H.); christian.spielmann@uni-jena.de (C.S.); mwz@berkeley.edu (M.Z.)
†These authors contributed equally to this work.

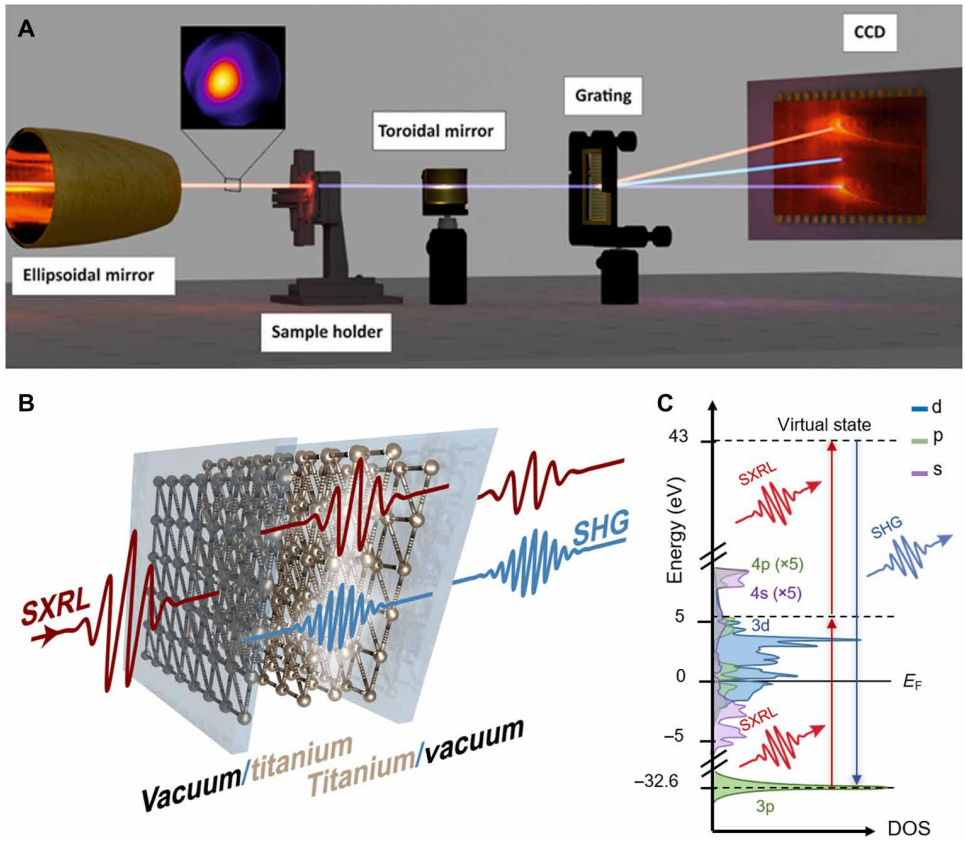

Fig. 1. Experimental setup and energy diagram for SXRL-SHG at the Ti $M_{2,3}$ edge. (**A**) From left, the setup includes the incoming 37.8-eV HHG-SXRL pulse (red beam, far-field beam profile in inset) that is focused by an ellipsoidal mirror onto the Ti foil surface, where SHG is generated (blue beam) and propagates collinearly with the fundamental. The divergent field is refocused with a toroidal mirror onto a grating that disperses the SHG and fundamental beams simultaneously onto a CCD camera. (**B**) Schematic diagram of the origin of the SHG emission. Inversion symmetry is broken on the front Ti surface, allowing for SHG. The fundamental and SHG beams exit from the rear foil surface. (**C**) Ti orbital-resolved density of states (DOS) (*40*). The SHG emission results from on-resonant excitation of 3p core states (−32.6 eV) to an empty intermediate state of 3d character (+5.2 eV) and subsequently to a virtual state (+43 eV).

(Fig. 1A, inset) was tightly focused using a Au-coated ellipsoidal mirror onto a Ti foil (hexagonal centrosymmetric, 6/*mmm* point group) placed at the rear focal plane of the ellipsoid with an on-target spot size of 4.5 ± 1.5 μm and average intensity of $4.1 \pm 1.9 \times 10^{11}$ W/cm^2 (Fig. 1B). Given the 50-nm thickness of the Ti foil and the estimated 13-nm attenuation depth of 37.8-eV photons in Ti (*25*), it is likely that the SHG signal was predominately generated on the front face of the foil, and SHG emission from the rear surface can be disregarded. These estimations are supported by the fact that measurements were also performed with 100-nm foils, for which no statistically significant SHG could be found, and by complementary DFPT simulations discussed below. Given that the SHG emission is confined to the Ti surface layer, the SHG emission is always phase-matched. Spectra recorded without the sample present lacked SHG signal between the 0th and ± 1st diffraction order, thus confirming that SHG emission was not a result of second harmonic contamination in incoming SXRL beam (fig. S2). This is an advantage of plasma-based sources as opposed to undulator based ones, since harmonic contributions to the incident beam are expected in the latter but not the former (*26*).

The on-target fluence of 0.7 ± 0.3 J/cm^2 surpassed the single-shot damage threshold as evidenced by consistent sample damage, which required moving the sample to an unexposed spot for each laser shot. Since the Ti conduction band (CB) consists primarily of 3d states, the 37.8-eV linear absorption can be attributed in part to a resonant dipole-allowed inter-shell transition from 3p core states to empty 3d CB states with SHG emerging from a subsequent transition to a virtual state 43 eV above the Fermi energy E_F (Fig. 1C).

The outgoing photons were refocused using a Au toroidal mirror and dispersed with a transmission grating (1000 lines/mm) onto a deep-cooled charge-coupled device (CCD; Princeton-MTE), enabling a simultaneous analysis of the fundamental and SHG peaks. The pulse energy was calibrated with respect to the counts on the CCD by measuring the shot-to-shot fluctuations of the SXRL and correlating the statistics with those observed on the CCD. A characteristic spectrum featuring the fundamental and SHG peaks is shown in Fig. 2A. Measurements of the seeded SXRL linewidth using a high-resolution spectrometer confirmed a linewidth at full width at half maximum of 2.6 meV, which is poorly resolved but expected since the spectrometer was optimized to cover more than one octave at low resolution to be sensitive for SHG. The broadened linewidth of the second harmonic is due to aberrations of the imaging spectrometer but otherwise expected to be the same order of magnitude as that of the fundamental. The background-corrected spectra were analyzed by integrating the peaks observed on the CCD and aggregating single-shot spectra according to the intensity of the

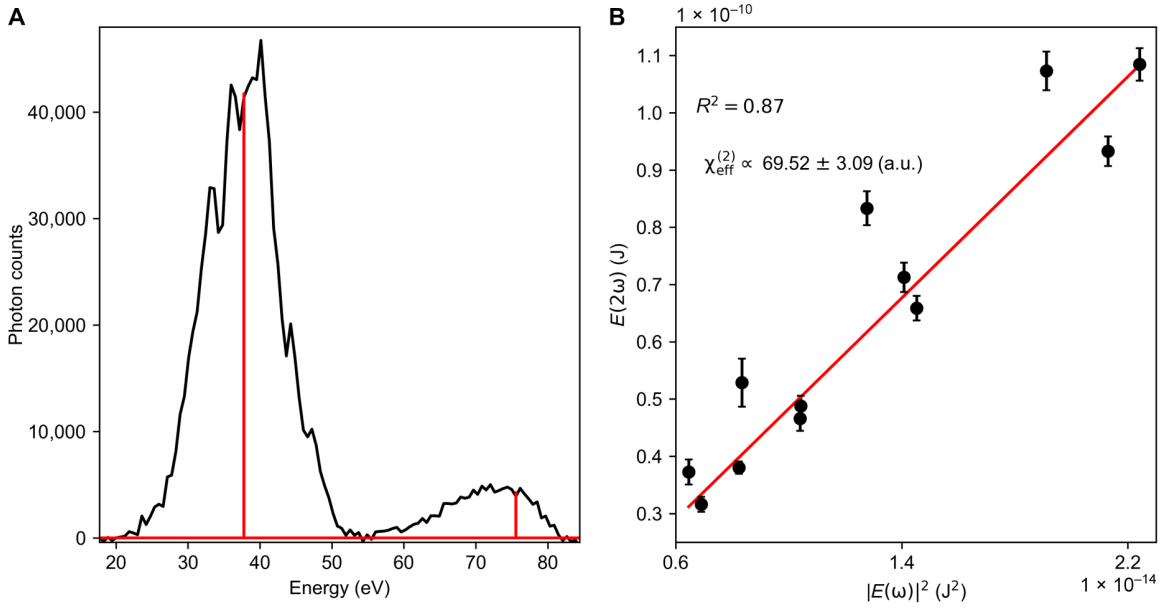

Fig. 2. Representative spectrum of fundamental and second harmonic peaks where the second harmonic response scales quadratically with that of the fundamental. (**A**) Representative spectrum of the fundamental and SHG signals (black). The linewidth is not resolved in this spectrum because of the spectrometer being optimized for high sensitivity exhibiting poor spectral resolution. The true linewidth of the SXRL was separately measured ($\Delta E \approx 2.6$ meV) with a high-resolution spectrometer (red line). The linewidth of the SHG signal is assumed to be of the same order of magnitude as that of the fundamental. (**B**) The nonlinear energy dependence of the SHG signal with respect to the fundamental. A linear equation (red line) is fit to experimental data plotted as $|E(\omega)|^2$ versus $E(2\omega)$ (black dots with 1 SD error bars, determined by the SD in photon counts on the CCD resulting from averaging shots at the same fundamental pulse energy together).

fundamental. The slope of a plot relating the on-target energies of the fundamental and SHG peaks allows retrieval of $\chi^{(2)}$ via Eq. 1 (Fig. 2B). To understand the SHG process in detail, first-principles DFPT (*27*) and RT-TDDFT calculations were performed using the *exciting* all-electron full-potential computer package using the formalism of Sharma and Ambrosch-Draxl (*28*) that uses linearized augmented planewave and local orbital methods, the results of which will be discussed below (*29*, *30*).

DISCUSSION

The quadratic modulo intensity dependence of the observed emission peak at 75.6 eV with respect to the energy of the fundamental (37.8 eV) was confirmed by a coefficient of determination (R^2) value of 0.87 (Fig. 2B) when plotting the incident pulse energies, $|E(\omega)|^2$ versus $E(2\omega)$. These results are in agreement with RT-TDDFT calculations performed using a development version of the SIESTA (*31*) electronic structure code. Here, a Ti slab was driven under an XUV monochromatic pulse to investigate its interaction with varying laser field intensity. The nonlinear second harmonic response was confirmed by fitting the current density, $J(2\omega)$, to a quadratic equation in the driving electric field strength (fig. S8). Hence, we ascribe the observed feature at 75.6 eV to a second-order nonlinear process involving frequency-doubling of the incoming SXRL beam. Using the mean yield of the SHG, fundamental, and input parameters of the SXRL, the SHG conversion efficiency was estimated to be $\eta = 0.023 \pm 0.005$.

Given the monochromaticity of the SXRL beam, it was not possible to measure the SHG spectrum across the Ti $M_{2,3}$ edge. However, linear absorption measurements performed with a table-top HHG source (Fig. 3) suggest that the efficiency of SHG at 37.8 eV could have a contribution from a resonantly-enhanced excitation process. From the linear absorption measurements, it can be seen that 37.8 eV lies well within the primary absorption feature due to the dipole-allowed 3p to 3d transition.

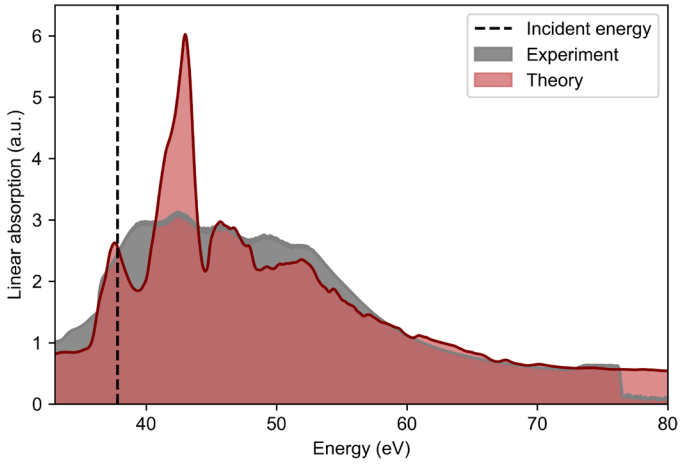

Fig. 3. The linear absorption spectrum from a broadband HHG source of the Ti foil. The experimentally measured onset of the Ti $M_{2,3}$ edge can clearly be seen (gray) and is confirmed by a calculated absorption spectrum (red). The incident energy used in the SHG experiment of 37.8 eV (black dashed line) lies well within the resonantly enhanced region of the absorption spectrum. a.u., arbitrary units.

Previous FEL experiments estimated a threshold power for nonlinear effects in the hard x-ray regime exceeding 10^{16} W/cm^2 (*14*). In the SXR regime, efficient SHG at incident intensities of $\approx 10^{12}$ W/cm^2

was observed (*17*, *32*). Our results demonstrate efficient SHG with smaller intensities ($\approx 10^{11}$ W/cm^2). The relatively lower intensities required here for SHG as opposed to those in the SXR regime could be due to the fewer number of K-shell electronic states and the weaker coupling of dipole moments between K-shell and valence electrons (*17*, *18*). Although beyond the scope of this first experimental work in the XUV, it appears worthwhile to explore how the nonlinear conversion efficiencies scale with the energies of core states in future theoretical work.

As for the surface specificity of this technique, DFPT calculations performed within the dipole approximation of the nonlinear susceptibility across the Ti $M_{2,3}$ edge find a bulk response more than nine orders of magnitude smaller than that originating from the surface (fig. S9). These results agree with symmetry considerations that predict SHG exclusively from the surface given that the vacuum-sample interface is noncentrosymmetric, while the bulk is not. This disparity in contributions points to the possibility that measuring relative differences in XUV-SHG emission after altering the surface chemistry of a centrosymmetric sample would be an element-specific probe of a changing surface environment.

In conclusion, we have shown the first successful demonstration of XUV-SHG with surface specificity indicated by first-principles calculations and performed nonlinear spectroscopy on a table-top SXRL system. In contrast with the energies required for SHG at FEL sources, it was possible that a table-top SXRL with nanojoule input energies and tight focusing could generate second harmonic radiation at 75.6 eV. In addition, the large number of transition metal elements with M edges in the XUV window potentially makes XUV-SHG a feasible technique for investigating the intrinsic properties of transition metal molecular complexes, heterojunctions, interfaces, and noncentrosymmetric materials with elemental specificity. The findings presented here hint at opportunities to perform time-resolved femtosecond or even attosecond nonlinear XUV spectroscopy experiments using, for example, the high-energy, wavelength-tunable XUV-HHG–based sources at the Extreme Light Infrastructure (*33*), up-scalable sources based on relativistic surface harmonics (*34*), or even broadband attosecond HHG-based table-top sources (*35*–*37*). With a small focus, peak intensities using the latter have reached 10^{14} W/cm^2 and have demonstrated two-photon absorption in atoms and molecules (*38*). Our first demonstration of nonlinear XUV spectroscopy on the table-top holds great promise to expand the nonlinear suite to tunable XUV-SFG to record broadband surface and interface spectra and reduce the temporal resolution by using few-femtosecond compressed optical gate pulses.

MATERIALS AND METHODS

The goal of the experiment was to measure SHG from a Ti surface at an SXRL. The linear XUV absorption spectrum was first measured with a broadband table-top HHG source to confirm the location of the Ti $M_{2,3}$ edge. A sub-4-fs, broadband NIR (near infrared) pulse centered at 730-nm was focused into an Ar gas jet, producing high harmonics. The linear absorption spectrum was collected by measuring the broadband XUV transmission through vacuum (T_{vac}) and through a 50-nm-thick Ti foil (T_{Ti}). Sets of these two measurements were repeated 127 times to determine the average absorbance $A = -\log(T_{Ti}/T_{vac})$.

The SHG measurements were subsequently conducted at the Laboratoire d'Optique Appliquée using the Salle Jaune Ti:Sapphire laser system (*24*), which delivers three independently compressed multiterawatt femtosecond pulses at a repetition rate of 10 Hz. The SXRL works by coupling a resonant HHG pulse into an SXR amplifier. The amplifier is a plasma of Kr^{8+} ions emitting at the $3d^9 4d_{(J=0)} \rightarrow 3d^9 4p_{(J=1)}$ transition at 32.8-nm (37.8-eV) generated by optical field ionization of a high-density Kr gas jet by an ultrashort infrared pump pulse (1.5 J, 30-fs, focused at 3×10^{18}W/cm^2). As a result of the high electron density of the plasma (up to 10^{20} e$^-$/cm^3), the pump pulse cannot propagate in the plasma. A waveguide was therefore implemented beforehand by focusing a 0.7-J, 0.6-ns infrared pulse in the gas jet using an axicon lens (*39*). The HHG was seeded with a 15-mJ, 30-fs infrared pulse focused in an Ar-filled gas cell and coupled into the Kr^{8+} amplifier using a grazing incidence toroidal mirror. The 25th harmonic of the HHG spectrum was tuned to the lasing transition by chirping the driver pulse, and the injection delay was set to 1.2 ps to match the SXRL gain peak position.

The SXRL was focused with an ellipsoidal mirror of a focal length of 33 cm (3-μm diffraction limit) onto the sample. An upper limit on the focal spot of 6-μm was estimated by the distance it required to move the position of the incident beam in the sample plane between laser shots because of the sample damage. The irradiated spot size was thus estimated be 4.5 ± 1.5 μm. To ensure that the sample plane was aligned with the focal position, the *z* position (optical axis) of the sample was varied until a threshold intensity strong enough to burn holes into the foil was reached. After hitting the sample, the fundamental and SHG beams were focused with a toroidal mirror (f = 33 cm) onto a cooled CCD camera (2048 × 2048 pixels of which a 1024 × 1024 quadrant was used because of the low pixel quality in the middle of the camera, pixel pitch of 13.5 μm, −50°C). A total of 394 spectra were recorded, 248 of which had full resolution of the CCD chip and 146 of which with a hardware binned camera of 2 × 2 pixels.

SUPPLEMENTARY MATERIALS

Supplementary material for this article is available at http://advances.sciencemag.org/cgi/content/full/7/21/eabe2265/DC1

REFERENCES AND NOTES

1. E. T. J. Nibbering, D. A. Wiersma, K. Duppen, Ultrafast nonlinear spectroscopy with chirped optical pulses. *Phys. Rev. Lett.* **68**, 514–517 (1992).
2. K. Tanaka, H. Hirori, M. Nagai, THz nonlinear spectroscopy of solids. *IEEE Trans. Terahertz Sci. Technol.* **1**, 301–312 (2011).
3. K. Tamasaku, E. Shigemasa, Y. Inubushi, I. Inoue, T. Osaka, T. Katayama, M. Yabashi, A. Koide, T. Yokoyama, T. Ishikawa, Nonlinear spectroscopy with x-ray two-photon absorption in metallic copper. *Phys. Rev. Lett.* **121**, 083901 (2018).
4. R. W. Boyd, *Nonlinear Optics (3rd Edition)* (Academic Press, 2008).
5. B. E. A. Saleh, M. C. Teich, *Fundamentals of Photonics* (John Wiley & Sons Inc., 1991).
6. P. B. Petersen, R. J. Saykally, On the nature of ions at the liquid water surface. *Annu. Rev. Phys. Chem.* **57**, 333–364 (2006).
7. Y. R. Shen, Surface properties probed by second-harmonic and sum-frequency generation. *Nature* **337**, 519–525 (1989).
8. K. B. Eisenthal, Liquid interfaces probed by second-harmonic and sum-frequency spectroscopy. *Chem. Rev.* **96**, 1343–1360 (1996).
9. Y. R. Shen, Optical second harmonic generation at interfaces. *Annu. Rev. Phys. Chem.* **40**, 327–350 (1989).
10. D. Hsieh, J. W. McIver, D. H. Torchinsky, D. R. Gardner, Y. S. Lee, N. Gedik, Nonlinear optical probe of tunable surface electrons on a topological insulator. *Phys. Rev. Lett.* **106**, 057401 (2011).
11. M. Dantus, Coherent nonlinear spectroscopy: From femtosecond dynamics to control. *Annu. Rev. Phys. Chem.* **52**, 639–679 (2001).
12. T. Yagasaki, S. Saito, Fluctuations and relaxation dynamics of liquid water revealed by linear and nonlinear spectroscopy. *Annu. Rev. Phys. Chem.* **64**, 55–75 (2013).
13. P. M. Kraus, M. Zürch, S. K. Cushing, D. M. Neumark, S. R. Leone, The ultrafast x-ray spectroscopic revolution in chemical dynamics. *Nat. Rev. Chem.* **2**, 82–94 (2018).

14. S. Shwartz, M. Fuchs, J. B. Hastings, Y. Inubushi, T. Ishikawa, T. Katayama, D. A. Reis, T. Sato, K. Tono, M. Yabashi, S. Yudovich, S. E. Harris, X-ray second harmonic generation. *Phys. Rev. Lett.* **112**, 163901 (2014).
15. S. Yamamoto, T. Omi, H. Akai, Y. Kubota, Y. Takahashi, Y. Suzuki, Y. Hirata, K. Yamamoto, R. Yukawa, K. Horiba, H. Yumoto, T. Koyama, H. Ohashi, S. Owada, K. Tono, M. Yabashi, E. Shigemasa, S. Yamamoto, M. Kotsugi, H. Wadati, H. Kumigashira, T. Arima, S. Shin, I. Matsuda, Element selectivity in second-harmonic generation of $GaFeO_3$ by a soft-x-ray free-electron laser. *Phys. Rev. Lett.* **120**, 223902 (2018).
16. E. Berger, S. Jamnuch, C. Uzundal, C. Woodahl, H. Padmanabhan, A. Amado, P. Manset, Y. Hirata, I. Matsuda, V. Gopalan, Y. Kubota, S. Owada, K. Tono, M. Yabashi, Y. Shi, C. Schwartz, W. Drisdell, J. Freeland, T. Pascal, M. Zuerch, Direct observation of symmetry-breaking in a 'ferroelectric' polar metal. arXiv:2010.03134 (2020).
17. R. K. Lam, S. L. Raj, T. A. Pascal, C. D. Pemmaraju, L. Foglia, A. Simoncig, N. Fabris, P. Miotti, C. J. Hull, A. M. Rizzuto, J. W. Smith, R. Mincigrucci, C. Masciovecchio, A. Gessini, E. Allaria, G. De Ninno, B. Diviacco, E. Roussel, S. Spampinati, G. Penco, S. Di Mitri, M. Trovò, M. Danailov, S. T. Christensen, D. Sokaras, T.-C. Weng, M. Coreno, L. Poletto, W. S. Drisdell, D. Prendergast, L. Giannessi, E. Principi, D. Nordlund, R. J. Saykally, C. P. Schwartz, Soft x-ray second harmonic generation as an interfacial probe. *Phys. Rev. Lett.* **120**, 023901 (2018).
18. C. P. Schwartz, S. L. Raj, S. Jamnuch, C. J. Hull, P. Miotti, R. K. Lam, D. Nordlund, C. B. Uzundal, C. D. Pemmaraju, R. Mincigrucci, L. Foglia, A. Simoncig, M. Coreno, C. Masciovecchio, L. Giannessi, L. Poletto, E. Principi, M. Zuerch, T. A. Pascal, W. S. Drisdell, R. J. Saykally, Ångström-resolved interfacial structure in organic-inorganic junctions. arXiv:2005.01905 (2020).
19. K. Midorikawa, Y. Nabekawa, A. Suda, XUV multiphoton processes with intense high-order harmonics. *Prog. Quantum Electron.* **32**, 43–88 (2008).
20. S. Sebban, A. Depresseux, E. Oliva, J. Gautier, F. Tissandier, J. Nejdl, M. Kozlova, G. Maynard, J. P. Goddet, A. Tafzi, A. Lifschitz, H. T. Kim, S. Jacquemot, P. Rousseau, P. Zeitoun, A. Rousse, Toward compact and ultra-intense laser based soft x-ray lasers. *Plasma Phys. Control. Fusion* **60**, 014030 (2018).
21. E. Takahashi, Y. Nabekawa, K. Midorikawa, Generation of 10-μJ coherent extreme-ultraviolet light by use of high-order harmonics. *Opt. Lett.* **27**, 1920–1922 (2002).
22. R. Klas, S. Demmler, M. Tschernajew, S. Hädrich, Y. Shamir, A. Tünnermann, J. Rothhardt, J. Limpert, Table-top milliwatt-class extreme ultraviolet high harmonic light source. *Optica* **3**, 1167–1170 (2016).
23. T. Helk, M. Zürch, C. Spielmann, Perspective: Towards single shot time-resolved microscopy using short wavelength table-top light sources. *Struct. Dyn.* **6**, 010902 (2019).
24. A. Depresseux, E. Oliva, J. Gautier, F. Tissandier, J. Nejdl, M. Kozlova, G. Maynard, J. P. Goddet, A. Tafzi, A. Lifschitz, H. T. Kim, S. Jacquemot, V. Malka, K. Ta Phuoc, C. Thaury, P. Rousseau, G. Iaquaniello, T. Lefrou, A. Flacco, B. Vodungbo, G. Lambert, A. Rousse, P. Zeitoun, S. Sebban, Table-top femtosecond soft x-ray laser by collisional ionization gating. *Nat. Photonics* **9**, 817–821 (2015).
25. B. L. Henke, E. M. Gullikson, J. C. Davis, X-ray interactions: Photoabsorption, scattering, transmission, and reflection at E = 50-30,000 eV, Z = 1-92. *At. Data Nucl. Data Tables* **54**, 181–342 (1993).
26. M. Fuchs, R. Weingartner, A. Popp, Z. Major, S. Becker, J. Osterhoff, I. Cortrie, B. Zeitler, R. Hörlein, G. D. Tsakiris, U. Schramm, T. P. Rowlands-Rees, S. M. Hooker, D. Habs, F. Krausz, S. Karsch, F. Grüner, Laser-driven soft-x-ray undulator source. *Nat. Phys.* **5**, 826–829 (2009).
27. P. Hohenberg, W. Kohn, Inhomogeneous electron gas. *Phys. Rev.* **136**, B864–B871 (1964).
28. S. Sharma, C. Ambrosch-Draxl, Second-harmonic optical response from first principles. *Phys. Scr.* **T109**, 128–134 (2004).
29. A. Gulans, S. Kontur, C. Meisenbichler, D. Nabok, P. Pavone, S. Rigamonti, S. Sagmeister, U. Werner, C. Draxl, Exciting: A full-potential all-electron package implementing density-functional theory and many-body perturbation theory. *J. Phys. Condens. Matter* **26**, 363202 (2014).
30. S. Sagmeister, C. Ambrosch-Draxel, Time-dependent density functional theory versus Bethe-Salpeter equation: An all-electron study. *Phys. Chem. Chem. Phys.* **11**, 4451–4457 (2009).
31. J. M. Soler, E. Artacho, J. D. Gale, A. García, J. Junquera, P. Ordejón, D. Sánchez-Portal, The SIESTA method for ab initio order-*N* materials simulation. *J. Phys. Condens. Matter* **14**, 2745–2779 (2002).
32. K. Yamamoto, Y. Kubota, M. Suzuki, Y. Hirata, K. Carva, M. Berritta, K. Takubo, Y. Uemura, R. Fukaya, K. Tanaka, W. Nishimura, T. Ohkochi, T. Katayama, T. Togashi, K. Tamasaku, M. Yabashi, Y. Tanaka, T. Seki, K. Takanashi, P. M. Oppeneer, H. Wadati, Ultrafast demagnetization of Pt magnetic moment in $L1_0$-FePt probed by magnetic circular dichroism at a hard x-ray free electron laser. *New J. Phys.* **21**, 123010 (2019).
33. I. Makos, I. Orfanos, A. Nayak, J. Peschel, B. Major, I. Liontos, E. Skantzakis, N. Papadakis, C. Kalpouzos, M. Dumergue, S. Kühn, K. Varju, P. Johnsson, A. L'Huillier, P. Tzallas, D. Charalambidis, A 10-gigawatt attosecond source for non-linear XUV optics and XUV-pump-XUV-probe studies. *Sci. Rep.* **10**, 3759 (2020).
34. O. Jahn, V. E. Leshchenko, P. Tzallas, A. Kessel, M. Krüger, A. Münzer, S. A. Trushin, G. D. Tsakiris, S. Kahaly, D. Kormin, L. Veisz, V. Pervak, F. Krausz, Z. Major, S. Karsch, Towards intense isolated attosecond pulses from relativistic surface high harmonics. *Optica* **6**, 280–287 (2019).
35. P. Tzallas, D. Charalambidis, N. A. Papadogiannis, K. Witte, G. D. Tsakiris, Direct observation of attosecond light bunching. *Nature* **426**, 267–271 (2003).
36. E. J. Takahashi, P. Lan, O. D. Mücke, Y. Nabekawa, K. Midorikawa, Attosecond nonlinear optics using gigawatt-scale isolated attosecond pulses. *Nat. Commun.* **4**, 2691 (2013).
37. F. Ferrari, F. Calegari, M. Lucchini, C. Vozzi, S. Stagira, G. Sansone, M. Nisoli, High-energy isolated attosecond pulses generated by above-saturation few-cycle fields. *Nat. Photonics* **4**, 875–879 (2010).
38. B. Manschwetus, L. Rading, F. Campi, S. Maclot, H. Coudert-Alteirac, J. Lahl, H. Wikmark, P. Rudawski, C. M. Heyl, B. Farkas, T. Mohamed, A. L'Huillier, P. Johnsson, Two-photon double ionization of neon using an intense attosecond pulse train. *Phys. Rev. A* **93**, 061402(R) (2016).
39. E. Oliva, A. Depresseux, M. Cotelo, A. Lifschitz, F. Tissandier, J. Gautier, G. Maynard, P. Velarde, S. Sebban, Hydrodynamic evolution of plasma waveguides for soft-x-ray amplifiers. *Phys. Rev. E* **97**, 023203 (2018).
40. A. Jain, S. P. Ong, G. Hautier, W. Chen, W. D. Richards, S. Dacek, S. Cholia, D. Gunter, D. Skinner, G. Ceder, K. A. Persson, Commentary: The Materials Project: A materials genome approach to accelerating materials innovation. *APL Mater.* **1**, 011002 (2013).
41. K. Yabana, G. F. Bertsch, Time-dependent local-density approximation in real time. *Phys. Rev. B Condens. Matter Mater. Phys.* **54**, 4484–4487 (1996).
42. G. F. Bertsch, J.-I. Iwata, A. Rubio, K. Yabana, Real-space, real-time method for the dielectric function. *Phys. Rev. B Condens. Matter Mater. Phys.* **62**, 7998–8002 (2000).
43. C. D. Pemmaraju, F. D. Vila, J. J. Kas, S. A. Sato, J. J. Rehr, K. Yabana, D. Prendergast, Velocity-gauge real-time TDDFT within a numerical atomic orbital basis set. *Comput. Phys. Commun.* **226**, 30–38 (2018).
44. Y. Takimoto, F. D. Vila, J. J. Rehr, Real-time time-dependent density functional theory approach for frequency-dependent nonlinear optical response in photonic molecules. *J. Chem. Phys.* **127**, 154114 (2007).
45. J. P. Perdew, A. Zunger, Self-interaction correction to density-functional approximations for many-electron systems. *Phys. Rev. B* **23**, 5048–5079 (1981).

Acknowledgments: We thank D. Attwood, C. Schwartz, C. Uzundal, and F. Tuitje for fruitful discussions. **Funding:** The research leading to these results has received funding from the European Community's Horizon 2020 research and innovation program under grant agreement no. 654148 (Laserlab Europe). M.Z. acknowledges support by the Max Planck Society (Max Planck Research Group) and the Federal Ministry of Education and Research (BMBF) under "Make our Planet Great Again - German Research Initiative" (grant no. 57427209 "QUESTforENERGY") implemented by DAAD. This work is supported by Investissements d'Avenir Labex PALM (ANR-10-LABX-0039-PALM). J.O. is supported by Basic Science Research Program through the National Research Foundation of Korea funded by the Ministry of Education (2019R1A6A3A03032979). H.-T.C. acknowledges support from the U.S. Air Force Office of Scientific Research nos. FA9550-19-1-0314 and FA9550-20-1-0334 and the W. M. Keck Foundation award no. 046300-002. This research used resources of the National Energy Research Scientific Computing Center, a DOE Office of Science User Facility supported by the Office of Science of the U.S. Department of Energy under contract no. DE-AC02-05CH11231. This work also used the Extreme Science and Engineering Discovery Environment (XSEDE), which is supported by NSF grant no. ACI-1548562. C.S. acknowledges support from the Deutsche Forschungsgemeinschaft (DFG; German Research Foundation) under Germany's Excellence Strategy–EXC 2051 (no. 390713860), "Balance of the Microverse." M.Z. acknowledges funding by the W. M. Keck Foundation (no. 993922), funding from the UC Office of the President within the Multicampus Research Programs and Initiatives (no. M21PL3263), and funding from Laboratory Directed Research and Development Program at Berkeley Lab (no. 107573). **Author contributions:** T.H., L.H., A.K., J.G., F.T., J.-P.G., S.S., and M.Z. performed the experiments. A.K., J.G., F.T., J.-P.G., and S.S. built, optimized, and operated the SXRL. A.K. performed detailed characterization of the SXRL and focus geometry. T.H., A.K., E.B., and M.Z. analyzed the data. S.J., C.D.P., and T.A.P. performed the simulations. J.O. and H.-T.C. performed linear absorption measurements. M.Z. conceived the experiment. C.S. and M.Z. supervised the project. T.H., E.B., and M.Z. wrote the manuscript with input from all authors. **Competing interests:** The authors declare that they have no competing interests. **Data and materials availability:** All data needed to evaluate the conclusions in the paper are available on the Dryad repository under DOI https://doi.org/10.6078/D1Z11P. Additional data related to this paper may be requested from the authors.

Submitted 2 September 2020
Accepted 30 March 2021
Published 19 May 2021
10.1126/sciadv.abe2265

Citation: T. Helk, E. Berger, S. Jamnuch, L. Hoffmann, A. Kabacinski, J. Gautier, F. Tissandier, J.-P. Goddet, H.-T. Chang, J. Oh, C. D. Pemmaraju, T. A. Pascal, S. Sebban, C. Spielmann, M. Zuerch, Table-top extreme ultraviolet second harmonic generation. *Sci. Adv.* **7**, eabe2265 (2021).

Table-top extreme ultraviolet second harmonic generation

Tobias Helk, Emma Berger, Sasawat Jamnuch, Lars Hoffmann, Adeline Kabacinski, Julien Gautier, Fabien Tissandier, Jean-Philipe Goddet, Hung-Tzu Chang, Juwon Oh, C. Das Pemmaraju, Tod A. Pascal, Stephane Sebban, Christian Spielmann and Michael Zuerch

Sci Adv **7** (21), eabe2265.
DOI: 10.1126/sciadv.abe2265